ACS chemical biology

Articles

pubs.acs.org/acschemicalbiology

Toxicity Modulation, Resistance Enzyme Evasion, and A-Site X-ray Structure of Broad-Spectrum Antibacterial Neomycin Analogs

Juan Pablo Maianti,[†] Hiroki Kanazawa,[‡] Paola Dozzo,[§] Rowena D. Matias,[§] Lee Ann Feeney,[§] Eliana S. Armstrong,[§] Darin J. Hildebrandt,[§] Timothy R. Kane,[§] Micah J. Gliedt,[§] Adam A. Goldblum,[§] Martin S. Linsell,[§] James B. Aggen,[§] Jiro Kondo,[‡] and Stephen Hanessian*[,†]

[†]Department of Chemistry, Université de Montréal, CP 6128 Succ. Centre-Ville, Montréal, Québec H3C3J7, Canada

[‡]Department of Materials and Life Sciences, Sophia University, 7-1 Kioi-cho, Chiyoda-ku, 102-8554 Tokyo, Japan

[§]Achaogen Inc., 7000 Shoreline Court, Suite 371, South San Francisco, California 94080, United States

Supporting Information

ABSTRACT: Aminoglycoside antibiotics are pseudosaccharides decorated with ammonium groups that are critical for their potent broad-spectrum antibacterial activity. Despite over three decades of speculation whether or not modulation of pK_a is a viable strategy to curtail aminoglycoside kidney toxicity, there is a lack of methods to systematically probe amine-RNA interactions and resultant cytotoxicity trends. This study reports the first series of potent aminoglycoside antibiotics harboring fluorinated N1-hydroxyaminobutyryl acyl (HABA) appendages for which fluorine-RNA contacts are revealed through an X-ray cocrystal structure within the RNA A-site. Cytotoxicity in kidney-derived cells was significantly reduced for the derivative featuring our novel β,β-difluoro-HABA group, which masks one net charge by lowering the pK_a without compromising antibacterial potency. This novel side-chain assists in evasion of aminoglycoside-modifying enzymes, and it can be easily transferred to impart these properties onto any number of novel analogs.

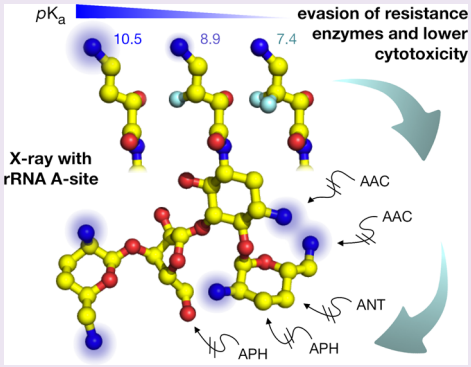

Aminoglycosides (AGs) comprise a diverse group of potent broad-spectrum natural and semisynthetic bactericidal antibiotics used in clinical practice worldwide.[1] AGs exploit the highly conserved A-site rRNA helix H44, at the core of the mRNA-tRNA decoding center of the bacterial 30S ribosomal subunit.[2−5] The binding of an AG to the A-site influences the bacterial ribosome to indiscriminately accept mismatched tRNAs while translating mRNA codons, which compromises the accuracy of protein synthesis.[2−6] Among the antibiotics that target the ribosome, only AGs possess broad-spectrum bactericidal activity against Gram-positive and Gram-negative bacteria,[7] and they are, in particular, highly effective against pathogens that cause life-threatening infections such as the ESKAPE group (*Escherichia coli*, *Staphylococcus aureus*, *Klebsiella* sp., *Acinetobacter* sp., *Pseudomonas aeruginosa*, and *Enterobacteriaceae* sp.).[1,8] AG antibiotics are subdivided into two classes based on the substitution pattern of the 2-deoxystreptamine core ring B (Figure 1).[1] The subclass of 4,5-disubstituted AGs includes the natural products neomycin (**1**), paromomycin (**2**), and butirosin (**3**).[1] Neomycin (**1**) is used in topical ointments,[9] while its 6′-hydroxyl congener paromomycin (**2**) is effective against leishmaniasis and dysenteric amoebiosis.[10] Butirosin (**3**) is a naturally occurring AG bearing a *N*1-(*S*)-hydroxy-aminobutyric acyl group (L-HABA),[11] a potentiating side-chain that has found wide application in

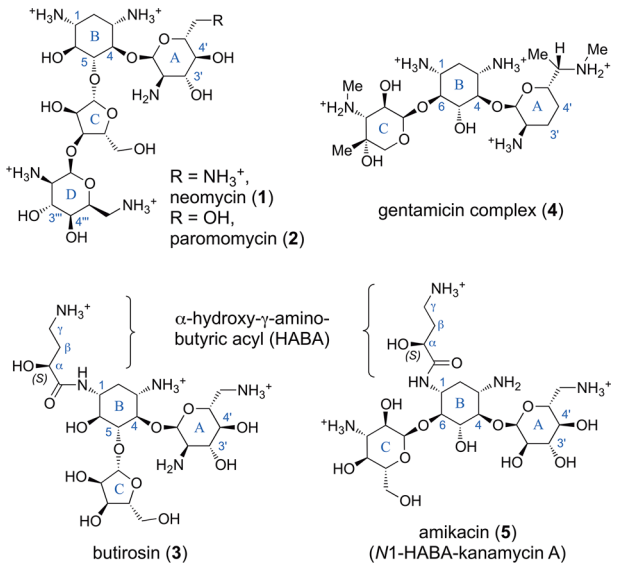

Figure 1. Representative AG antibiotics of 4,5- and 4,6-disubstited subclasses, and N1-substituted analogs.

Received: May 2, 2014
Accepted: July 1, 2014
Published: July 14, 2014

   dx.doi.org/10.1021/cb5003416 | *ACS Chem. Biol.* 2014, 9, 2067−2073

Scheme 1. Asymmetric Synthesis of β-Substituted HABA Derivatives and Synthesis of Tetradeoxy-Neomycin Analogs Featuring N_1−HABA Substituentsc Ranging Over 3 Orders of Magnitude in γ-N pK_a Values[29,30]

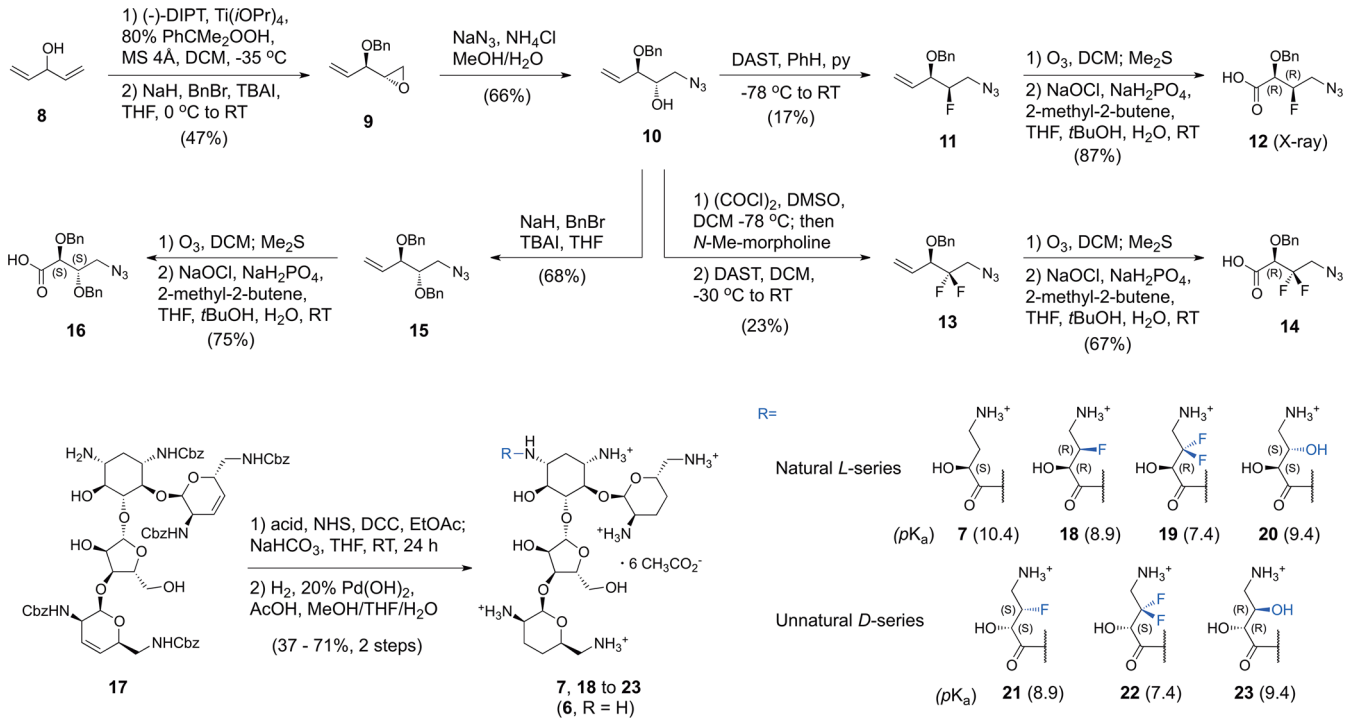

semisynthetic AG antibiotics (Figure 1).[1,12] The 4,6-disubstituted AG class includes clinically relevant natural products such as the gentamicin complex (**4**), tobramycin, and semisynthetic analogs such as amikacin (**5**), a kanamycin derivative with an appended *N*1-L-HABA chain (Figure 1).[1]

Selective pressure from medical and veterinary use of antibiotics has led to the evolution and dispersion of numerous aminoglycoside-modifying enzymes (AMEs) that undermine the effectiveness of clinically deployed antibiotics (Supporting Information Figure S1).[13−16] These enzymes target amine and hydroxyl groups in AGs and are accordingly classified *N*-acetyltransferases (AAC), *O*-phosphotransferases (APH), and *O*-adenyltransferases (ANT) (Supporting Information Table S1).[13−16] Other resistance mechanisms include efflux pumps and rRNA methyltransferases (ArmA) that abrogate target binding by all 4,6-disubstituted type AGs such as **4** and **5**.[1,17] Extensive efforts have been made over the years to advance to the clinic novel AG antibiotics that evade AME resistance mechanisms by semisynthetic deoxygenation of susceptible functionalities, such as the 3′ and 4′-hydroxyl groups, and also by appendage of the *N*1-L-HABA substituent that clashes with the active site pockets of multiple AMEs (Supporting Information Figure S1).[18−21] Because clinical AG antibiotics **1**−**5** and congeners of the 4,6-disubstituted AG class do not evade an important subset of AMEs (Supporting Information Figure S1),[13−16] our group has investigated a series of potent broad-spectrum semisynthetic neomycin and paromomycin analogs,[18−21] for example the novel antibiotic 3′,4′,3‴,4‴-tetradeoxy-neomycin **6** and its *N*1-L-HABA analog **7** (Scheme 1) capable of evading multiple AG-resistance mechanisms and modifying enzymes (Table 1, Supporting Information Figure S1).[20]

A long-standing challenge for medicinal chemists is to systematically improve the toxicity profiles of next-generation AG antibiotics without compromising their broad-spectrum antibacterial potency.[1,12,22,23] Kidney toxicity correlates with the number of protonated and nonprotonated amino groups on the AG sugar scaffolds,[24] yet these features are also a requirement for potent antibacterial action.[1,5] This prevailing model raises the possibility that modulation of the net charge of AG analogs at physiological pH could lead to improved therapeutic indexes.[1,22−24] However, despite many decades of speculation, this idea remains untested because of our lack of systematic methods to modulate AG net charge without concomitantly disrupting key target rRNA interactions (Supporting Information Figure S2).[1,12] These observations highlight the need to understand the relationship among antibacterial potency, cellular toxicity, and functionally relevant RNA contacts. Furthermore, structure−activity differentiation between the eukaryotic and prokaryotic ribosomal A-sites may be useful to curtail inner ear toxicity of AGs.[1,25−28] Herein, we report a generalizable strategy to shift the protonation state of the most basic amino group of AG analogs over 3 orders of magnitude of the pH scale (10.5 to 7.4), with broad implications for the development of potent and potentially less toxic next-generation AG antibiotics.

RESULTS AND DISCUSSION

We devised a divergent synthetic strategy to access a complete series of enantiopure β-substituted D- and L-HABA derivatives suitable for examination of potency and cytotoxicity trends. Precedent routes for the synthesis of HABA groups were unsuitable to access a difluoro substitution pattern,[29] which is required to lower the pK_a of ammonium groups to the range of physiological pH.[30] Our strategy required functionalities and protecting groups compatible with the fluorination reagent diethylaminosulfur trifluoride (DAST),[31] such as *O*-benzyl and azide groups, while the carboxylic acid was latently masked as an olefin until a later stage (Scheme 1). Our retrosynthetic analysis (Supporting Information Figure S3) brought us to

dx.doi.org/10.1021/cb5003416 | ACS Chem. Biol. 2014, 9, 2067−2073

Table 1. Minimum Inhibitory Concentration (MIC, μg/mL) Against ESKAPE Strains Expressing AMEs

entry	MIC values (μg/mL) bacterium/enzyme	NeoB (1)	Par (2)	Gent (4)	Amk (5)	6	7	18	19	20	21	22	23
1	*E. coli*[a]	2	4	0.5	2	0.5	0.5	0.5	0.5	1	1	4	2
2	*S. aureus*[b]	0.5	2	0.5	2	0.5	0.5	0.5	0.5	0.5	0.5	1	0.5
3	*K. pnuemoniae*[c]	0.5	2	0.25	0.5	0.5	0.5	0.5	0.5	0.5	0.5	2	1
4	*A. baumannii*	1	4	2	2	0.25	1	0.5	0.5	0.5	0.5	2	1
5	*P. aeruginosa*[d] APH(3′)	32	>64	0.5	2	0.25	0.5	0.5	1	0.5	1	4	1
6	*E. cloacae,* APH(3′)-I, ANT(2″)-I, AAC(6′)	>64	>64	32	64	>64	4	2	2	2	4	32	16
7	*E. coli* APH(3′)-Ib	64	>64	0.25	0.5	32	0.25	0.25	0.25	0.5	1	4	2
8	*S. aureus* APH(3′/5″)-III	>64	>64	0.5	8	32	1	1	1	1	1	4	2
9	*A. baumannii,* AAC(3)-I, APH(3′)-VI, ANT(2″)-I	>64	>64	>64	>64	32	2	1	2	2	2	8	2
10	*S. aureus* ANT(4′)-I	>64	>64	0.5	64	0.5	1	1	2	1	1	4	2
11	*P. aeruginosa* ANT(4′)-II	8	>64	2	32	1	1	1	2	1	2	16	2
12	*E. coli* ANT(2″)-I	2	4	64	4	2	2	2	2	2	2	8	8
13	*P. aeruginosa* AAC(6′)-II	8	>64	32	4	2	1	1	2	1	2	16	2
14	*S. aureus* AAC(6′)/APH(2″)	>64	>64	>64	64	>64	2	2	4	2	8	16	8
15	*E. coli* AAC(3)-IV	2	8	16	2	2	2	1	1	1	4	8	2
16	*E. coli* rRNA methyltransferase ArmA	1	4	>64	>64	1	1	0.5	1	1	2	4	2

Strains were obtained from ATCC: [a]ATCC 25922, [b]ATCC 29213, [c]ATCC 10031, [d]ATCC 27853. Abbreviations: NeoB, neomycin B (**1**); Par, paromomycin (**2**); Gent, gentamicin-C complex (**4**); Amk, amikacin (**5**).

divinyl-carbinol (**8**) as an ideal precursor for divergent asymmetric synthesis. In practice, **8** was desymmetrized using the Sharpless epoxidation procedure with the ligand (−)-diisopropyl-tartrate (DIPT),[32] followed by benzylation to yield enantiopure epoxide **9** (99% ee, chiral gas chromatography). Similarly, we used (+)-DIPT to access an "unnatural" series of D-HABA chains for comparative cytotoxicity studies (Scheme 1). Subsequently, epoxide **9** was opened using ammonium azide to afford **10** as a single diastereomer. The azido alcohol intermediate **10** was divergently elaborated to produce the β-substituted and β,β-disubstituted γ-azido-L-HABA derivatives **12**, **14**, and **16** in 3−4 steps and 15−51% overall yield (Scheme 1). The relative and absolute stereochemistries for (*R*,*R*)-**12** and the enantiomer (*S*,*S*)-**ent-12** were verified by X-ray crystallography (Supporting Information Figure S4). To our knowledge, this is the first successful fluorination strategy to access the challenging β,β-difluorinated L-HABA motif.[29]

With a series of seven HABA derivatives in hand, comprising *N*-Cbz-HABA and azide-protected natural and unnatural enantiomers of **12**, **14**, and **16**, we were poised for amide coupling to a suitable AG scaffold. We selected tetradeoxy-neomycin **6** selectively protected as intermediate **17**, which we previously reported in the synthesis of antibiotic **7**.[20] This intermediate can be produced in four steps and in excellent yield from neomycin (**1**), employing a diol-selective deoxygenation procedure followed by selective N1 deprotection via a base-labile *N*1,*O*6-oxazolidinone (Supporting Information Figure S3).[20] For the coupling reaction, the acyl chains were activated as *N*-hydroxysuccinimide esters[29] (Scheme 1). The corresponding N1-acyl products were obtained in 52−91% yield after chromatographic purification, then subjected to global hydrogenolytic deprotection with concomitant reduction of azide and olefins using Pearlman's catalyst (20% $Pd(OH)_2$/C) in yields ranging from 52 to 87% (Scheme 1). The final analogs **18** to **23** were purified by silica gel column chromatography eluted with ammonia/MeOH/$CHCl_3$,[18−21] and they were evaluated using NMR spectroscopy (^1H, ^{13}C, and ^{19}F), and using Charged Aerosol Detection HPLC, which indicated purities >90 to 95% (Supporting Information).

Potency and Evasion of Resistance Mechanisms. To examine the effects of γ-N pK_a modulation on antibacterial potency we compared the minimum inhibitory concentration (MIC) of clinical antibiotics with the novel analogs against a broad panel of susceptible and resistant strains of ESKAPE pathogens (Table 1). The resulting MIC values for the β-substituted L-HABA analogs **18** to **20** against wild-type strains were in the range 0.5−2.0 μg/mL (Table 1, entries 1−5), essentially indistinguishable from the parent analog **7**. Remarkably, excellent antibacterial potency was also maintained throughout the panel of AG-resistant strains (Table 1, entries 6−16, and Supporting Information Figure S1).

Analogs **18** to **20** display improved MICs values over neomycin B (**1**), gentamicin (**4**), amikacin (**5**), and tetradeoxy-neomycin (**6**) against the collection of ESKAPE strains (Table 1). In particular, the clinical AG antibiotics are ineffective against corresponding subsets of strains expressing AMEs (MIC ranges 16 to >64 μg/mL, Table 1, see Supporting Information Figure S1 for summary).[13−16] Comparing the MIC values for the unsubstituted tetradeoxy-neomycin analog **6** (Scheme 1, Table 1) reveals the broad-spectrum potentiation and enhanced evasion of AMEs conferred by the combination of 3′,4′-dideoxygenation and N1-acylation displayed by the analogs **7**, **18**, **19**, and **20** (Table 1).

By contrast, the series of control D-HABA analogs (**23**−**25**) produced relatively weaker antibacterial activities, displaying a strong correlation with γ-N pK_a (Table 1). For example, the pair of monofluoro analogs **18** and **21** produced comparable MIC values, whereas the difluoro congener **22** revealed a major discrepancy in potency with analog **19**. These data suggest both D- or L-β,β-difluoro-HABA substituents effectively influence the γ-amine net charge at physiological pH,[30] a point at which isosteric modifications become essential to maintain antibiotic potency.

X-ray Cocrystal Structural Studies. The potentiating effect of N1-HABA substituents on AG antibiotics has been extensively documented but remains poorly understood.[18,33] We speculated on the possibility that introduction of a *threo*-fluorine atom on HABA groups (**12** and **14**) could potentially alter the binding mode of these side-chains on our novel AG analogs. To investigate these interactions we solved the X-ray

dx.doi.org/10.1021/cb5003416 | ACS Chem. Biol. 2014, 9, 2067−2073

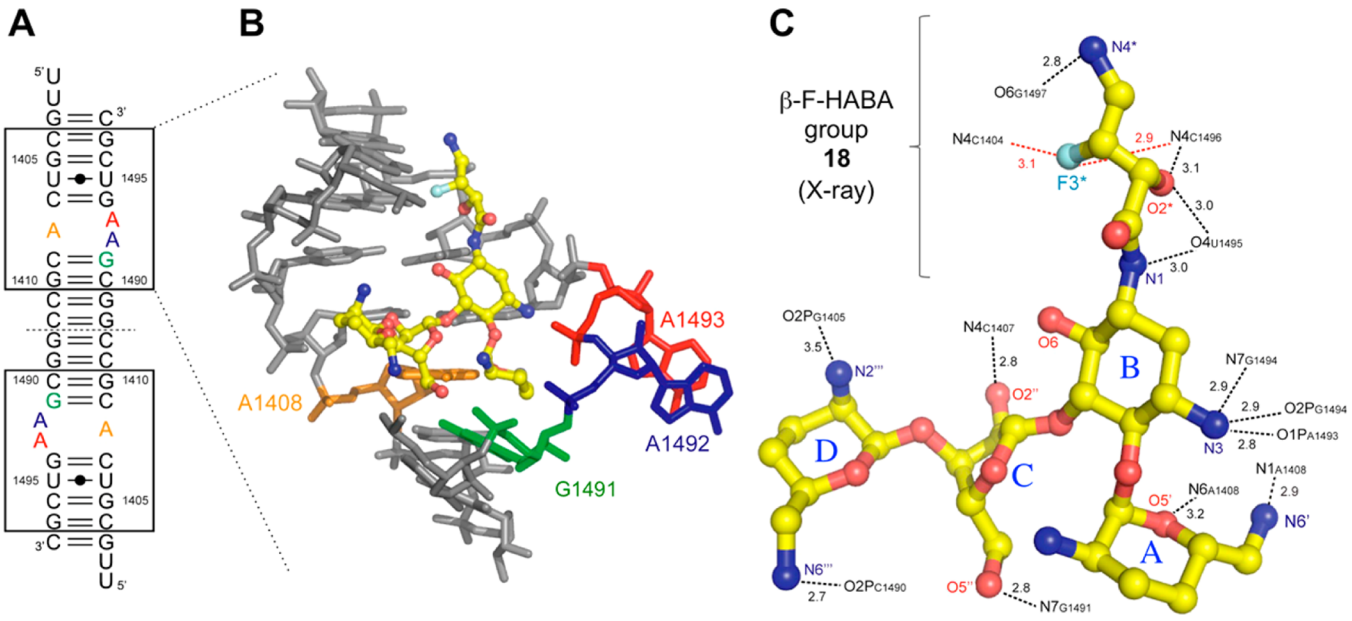

Figure 2. (A) Oligonucleotide comprising two palindromic A-site models (boxes), key functional residues are color-coded, numbering is for *E. coli* rRNA. (B) Co-crystal of **18** within the A-site RNA (see also Supporting Information Figure S5). (C) H-bond interactions of **18** with RNA (dashed lines). The *threo*-fluorine of **18** displays interactions with the Hoogsteen faces of C1404 and C1496 (red dashes).

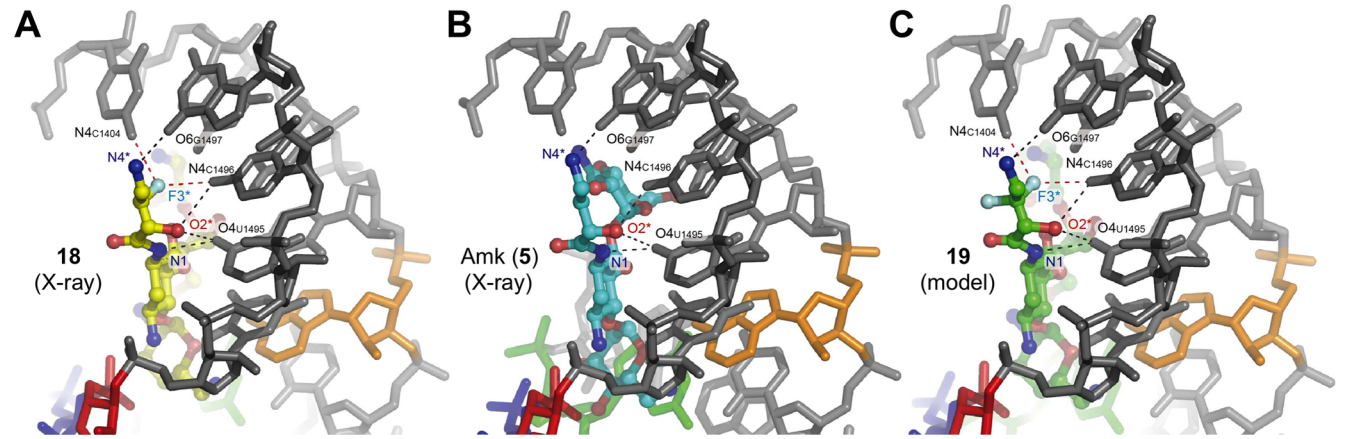

Figure 3. Conserved A-site RNA cocrystal interactions with the HABA groups of (A) analog **18**, (B) amikacin (**5**),[33] and (C) predicted placement of the second fluorine of **19** (see Supporting Information Figures S6 and S7 for more comparisons).

cocrystal structure of **18** within the A-site RNA binding site (Figure 2, Supporting Information Tables S2−3). We observed the placement of the AG sugar backbone is essentially superimposable to that of paromomycin within the 30S ribosome X-ray structure (Supporting Information Figure S5) indicating that the A-site model (Figure 2B) is faithful to the larger ribosome structure.[2] Furthermore, the placement of the fluorinated N1-HABA group and the H-bond interaction network (Figure 2C) are essentially identical to those observed for amikacin (**5**) in the A-site (Figure 3A-B), as well as a doubly functionalized paromomycin analog reported by our group (Supporting Information Figure S6).[18,33] Importantly, the *threo*-fluorine atom is accommodated by making halogen-H-bond contacts with the Hoogsteen faces of N4(C1404) and N4(C1496). This model predicts that the second *erythro*-fluorine substitution of **19** can be accommodated by pointing away from the RNA (Figure 3C). A detailed study of the X-ray structure (Supporting Information Figure S7) suggests that only perfectly isosteric L-HABA appendages are able to preserve all the rRNA interactions that endow optimum potency, consistent with the comparable antibiotic activity of analogs **7**, **18**, **19**, and **20** (Table 1). The novel *β*,*β*-difluoro-L-HABA chain of **19** enables unprecedented modulation of the *γ*-N pK_a, effectively neutralizing its charge at physiological pH, and displays excellent broad-spectrum potency by precluding inactivation by AMEs as effectively as cationic HABA groups (Table 1).

Modulation of Kidney Cell Toxicity. Next, we examined the cytotoxic potential of our analogs by measuring induction of cell death in the human kidney cell line HK2.[34] Kidney cells are the standard model for studying cytotoxicity mechanisms, because they actively accumulate AGs and subsequently elicit concentration-dependent activation of apoptosis through the caspase-3/7 intrinsic pathway.[24,35,36] The effective AG concentration for 50% (EC_{50}) activation of caspases 3/7 was measured using a luminescence based assay (Figure 4).[34] Our results for both the L- and D-stereochemical series suggest that the HABA analogs of highest *γ*-N pK_a elicited apoptosis with an average

dx.doi.org/10.1021/cb5003416 | ACS Chem. Biol. 2014, 9, 2067−2073

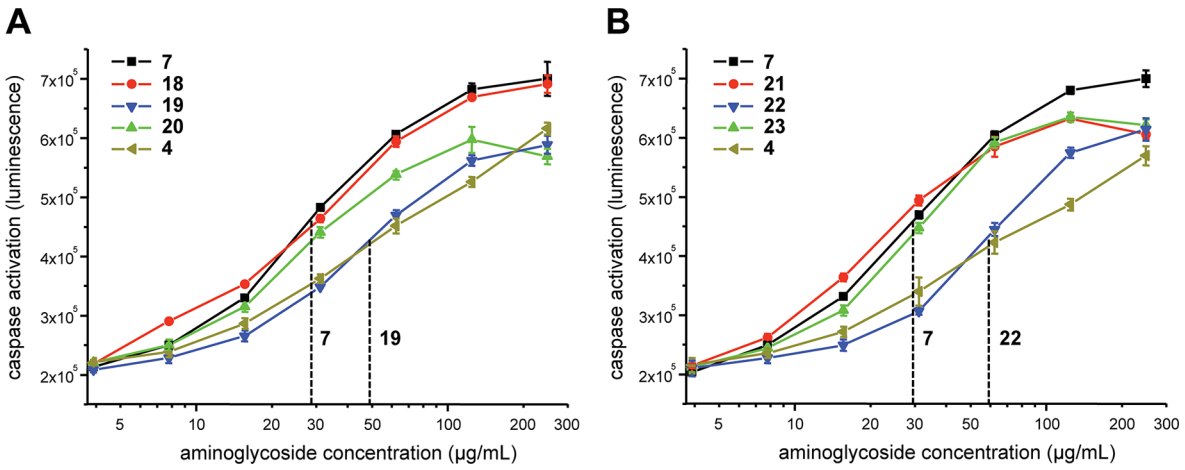

Figure 4. Apoptosis assay of human kidney cell line HK2 exposed to β-substituted N_1-HABA analogs of (A) natural L-series or (B) unnatural D-series. The parent N_1-HABA-tetradeoxy-neomycin **7** was used for comparison. Gentamicin (**4**) was included as assay control. Dotted lines indicate the EC_{50} value of the parent analog 7 and the β,β-difluoro-N_1–HABA analogs **19** and **22**.

EC_{50} = 26 μg/mL and were indistinguishable with the parent analog **7** within assay error (EC_{50} = 28 μg/mL). By contrast, the β,β-difluoro HABA analogs **19** and **22** required approximately 2-fold higher concentrations to elicit apoptosis (EC_{50} = 47 and 58 μg/mL, respectively). The disconnect between MIC potency and apoptosis trends are consistent with the reported mechanism of AG cytotoxicity that is independent of cellular ribosomes.[24,35,36] These results suggest that the novel β,β-difluoro-L-HABA derivatives with reduced γ-N pK_a were better tolerated by kidney cells compared to the parent analog **7** or isosteric congeners of higher pK_a (Figure 4). These observations are also supported by comparing calculated area under the curves (AUC) for the concentration-dependent apoptotic responses (Supporting Information Figure S8), as well as complementary cell viability assays (Supporting Information Figure S9).

Conclusions. Taken together, the broad-spectrum antibacterial *in vitro* activity coupled with the lower kidney cell toxicity bodes well for neomycin analogs such as **19** as new generation aminoglycosides with high therapeutic potential. This study provides the first demonstration of a systematic reduction in kidney cell toxicity using difluorination as a means to modulate basicity in the AG antibiotics. The novel β,β-difluoro-L-HABA side-chain is designed to maximize and preserve stabilizing A-site interactions, endowing potent broad-spectrum bactericidal activity against Gram-positive and Gram-negative bacteria, including ESKAPE group pathogens expressing multiple resistance mechanisms. Our findings suggest the antibacterial potentiation and toxicity-lowering features of the β,β-difluoro-L-HABA derivative may translate to numerous semisynthetic analogs, which has implications for the development of a safer next generation of AG antibiotics.

METHODS

Extended experimental and chemical synthesis procedures are found in the Supporting Information file.

Apoptosis and Viability Assays. Human kidney proximal tubule HK-2 cells (ATCC CRL-2190) were cultured in keratinocyte serum-free medium (KSFM) supplemented with 5 ng/mL epidermal growth factor (EGF), and 50 μg/mL bovine pituitary extract (BPE). Cells were maintained at subconfluence, and when they reached 80% confluence, they were washed with Dulbecco's PBS buffer (Invitrogen), harvested by treatment with trypsin-EDTA (Invitrogen) for ~1 min, and dispensed into a clear-bottom 96-well polystyrene tissue-culture plate (EK-25098, E&K Scientific) at a density of 1.6 × 10^4 cells/well in a final volume of 100 μL. The plates were incubated at 37 °C with 5% CO_2 for 3 days. Plates were removed from the incubator and the media was removed using a multichannel aspirator. Test compounds were serially diluted in KSFM medium containing 20 mM HEPES buffer. The compound solutions were prewarmed when added to plates, and then returned to incubation at 37 °C for 31 h. Blanks without cells and negative controls without compound were included. A serial dilution curve for gentamicin was included as an assay control.

For caspase-3/7-activation assays, following incubation, the plates were equilibrated at RT for 30 min, and added 50 μL of Caspase-Glo reagent (Promega) to each well. The plates were briefly agitated on a shaker platform, and incubated at RT for 30 min. Luminescence was measured using the luminometer Analyst HT (LJL Biosystems, 482 nm, 0.100 s integration). Area under the curve was calculated using the trapezoid area equation.

For cell viability assays, following incubation, the plates were equilibrated at RT, and 100 μL of CellTiter-Glo reagent (Promega) was added to each well. The plates were agitated on a shaker platform for 2 min, incubated at RT for 10 min, and followed by luminescence measurements.

Antibacterial Assays. MICs were determined using the standard serial dilution method, as previously described.[18−21] AME genes and resistance mechanisms in the Achaogen Strain Collection have been confirmed by PCR.[18−21]

Crystallization and Structure Determination. The A-site model RNA oligomer was chemically synthesized (Dharmacon, Boulder, CO), purified by 20% denaturing polyacrylamide gel electrophoresis and desalted by reversed-phase chromatography. Plate-shaped crystals of the RNA in complex with antibiotic **18** (A-site•**18**) were obtained using condition described in Supporting Information Table S2. An X-ray data set of A-site•**18** was collected at 100 K with synchrotron radiation at the structural biology beamlines BL-5A in the Photon Factory (Tsukuba, Japan). The data set was processed with the program *CrystalClear* (Rigaku/MSC). The obtained intensity data were further converted to structure-factor amplitudes using *TRUNCATE* from the *CCP4* suite. The statistics of data collection and the crystal data are summarized in Supporting Information Table S3. The initial phase of A-site•**18** was solved with the molecular replacement program *AutoMR* from the *Phenix* suite using the coordinate of the bacterial A-site in complex with tobramycin (PDB code: 1LC4). The molecular structure was constructed and manipulated with the programs *Coot*. The atomic parameters of the structure were refined with the program *CNS* through a combination of simulated-annealing, crystallographic conjugate gradient minimiza-

dx.doi.org/10.1021/cb5003416 | *ACS Chem. Biol.* 2014, 9, 2067−2073

tion refinements and *B*-factor refinements. The statistics of structure refinement are summarized in Supporting Information Table S3. Molecular drawings were made using *PyMOL*.

■ ASSOCIATED CONTENT

Supporting Information

Figures S1−S8, Tables S1−S3, experimental procedures, X-ray coordinate files, full spectroscopic data, GC and HPLC reports. This material is available free of charge via the Internet at http://pubs.acs.org.

Accession Codes

The atomic coordinates for the A-site•**18** complex have been deposited in the Protein Data Bank (PDB) with the ID code 3WRU.

■ AUTHOR INFORMATION

Corresponding Author

*Email: stephen.hanessian@umontreal.ca.

Notes

The authors declare no competing financial interest.

■ ACKNOWLEDGMENTS

This work was supported by the Achaogen Research Chair and the Natural Sciences and Engineering Research Council of Canada (NSERC). J.P.M. received fellowship support from Fonds de Recherche en Santé du Québec (FRSQ). J.K. was supported by a Grant-in-Aid for Young Scientists (23790054) from the Ministry of Education, Culture, Sports, Science and Technology, Japan. We acknowledge the Photon Factory synchrotron radiation facilities (No. 2012G519) and the BL-5A beamline staff. We thank Dr. Deschênes-Simard for X-ray structure analysis of **12** and **ent-12**.

■ REFERENCES

(1) Arya, D. P. (2007) *Aminoglycoside Antibiotics: From Chemical Biology to Drug Discovery*, Wiley-Interscience, Hoboken, NJ.

(2) Carter, A. P., Clemons, W. M., Brodersen, D. E., Morgan-Warren, R. J., Wimberly, B. T., and Ramakrishnan, V. (2000) Functional insights from the structure of the 30S ribosomal subunit and its interactions with antibiotics. *Nature 407*, 340−348.

(3) Wimberly, B. T., Brodersen, D. E., Clemons, W. M., Jr., Morgan-Warren, R. J., Carter, A. P., Vonrhein, C., Hartsch, T., and Ramakrishnan, V. (2000) Structure of the 30S ribosomal subunit. *Nature 407*, 327−339.

(4) Ogle, J. M., and Ramakrishnan, V. (2005) Structural insights into translational fidelity. *Annu. Rev. Biochem. 74*, 129−177.

(5) Francois, B., Russell, R. J., Murray, J. B., Aboul-ela, F., Masquida, B., Vicens, Q., and Westhof, E. (2005) Crystal structures of complexes between aminoglycosides and decoding A-site oligonucleotides: Role of the number of rings and positive charges in the specific binding leading to miscoding. *Nucleic Acids Res. 33*, 5677−5690.

(6) Wilson, D. N. (2009) The A−Z of bacterial translation inhibitors. *Crit. Rev. Biochem. Mol. Biol. 44*, 393−433.

(7) Kohanski, M. A., Dwyer, D. J., and Collins, J. J. (2010) How antibiotics kill bacteria: From targets to networks. *Nat. Rev. Microbiol. 8*, 423−435.

(8) Boucher, H. W., Talbot, G. H., Bradley, J. S., Edwards, J. E., Gilbert, D., Rice, L. B., Scheld, M., Spellberg, B., and Bartlett, J. (2009) Bad bugs, no drugs: no ESKAPE! An update from the Infectious Diseases Society of America. *Clin. Infect. Dis. 48*, 1−12.

(9) Waksman, S. A., Lechevalier, H. A., and Harris, D. A. (1949) Neomycin: Production and antibiotic properties. *J. Clin. Invest. 28*, 934−939.

(10) Davidson, R. N., den Boer, M., and Ritmeijer, K. (2009) Paromomycin. *Trans. R. Soc. Trop. Med. Hyg. 103*, 653−660.

(11) Howells, J. D., Anderson, L. E., Coffey, G. L., Senos, G. D., Underhill, M. A., Vogler, D. L., and Ehrlich, J. (1972) Butirosin, a new aminoglycosidic antibiotic complex: Bacterial origin and some microbiological studies. *Antimicrob. Agents Chemother. 2*, 79−83.

(12) Price, K. E. (1986) Aminoglycoside research 1975−1985: Prospects for development of improved agents. *Antimicrob. Agents Chemother. 29*, 543−548.

(13) Shaw, K. J., Rather, P. N., Hare, R. S., and Miller, G. H. (1993) Molecular genetics of aminoglycoside resistance genes and familial relationships of the aminoglycoside-modifying enzymes. *Microbiol. Rev. 57*, 138−163.

(14) Mingeot-Leclercq, M. P., Glupczynski, Y., and Tulkens, P. M. (1999) Aminoglycosides: Activity and resistance. *Antimicrob. Agents Chemother. 43*, 727−737.

(15) Azucena, E., and Mobashery, S. (2001) Aminoglycoside-modifying enzymes: Mechanisms of catalytic processes and inhibition. *Drug Resist. Updates 4*, 106−117.

(16) Magnet, S., and Blanchard, J. S. (2005) Molecular insights into aminoglycoside action and resistance. *Chem. Rev. 105*, 477−498.

(17) Paulsen, I. T., Brown, M. H., and Skurray, R. A. (1996) Proton-dependent multidrug efflux systems. *Microbiol. Rev. 60*, 575−608.

(18) Kondo, J., Pachamuthu, K., Francois, B., Szychowski, J., Hanessian, S., and Westhof, E. (2007) Crystal structure of the bacterial ribosomal decoding site complexed with a synthetic doubly functionalized paromomycin derivative: A new specific binding mode to an A-minor motif enhances *in vitro* antibacterial activity. *ChemMedChem 2*, 1631−1638.

(19) Hanessian, S., Pachamuthu, K., Szychowski, J., Giguère, A., Swayze, E. E., Migawa, M. T., François, B., Kondo, J., and Westhof, E. (2010) *Bioorg. Med. Chem. Lett. 20*, 7097−7101.

(20) Hanessian, S., Giguère, A., Grzyb, J., Maianti, J. P., Saavedra, O. M., Aggen, J. B., Linsell, M. S., Goldblum, A. A., Hildebrandt, D. J., Kane, T. R., Dozzo, P., Gliedt, M. J., Matias, R. D., Feeney, L. A., and Armstrong, E. S. (2011) Toward overcoming *Staphylococcus aureus* aminoglycoside resistance mechanisms with a functionally designed neomycin analogue. *ACS Med. Chem. Lett. 2*, 924−928.

(21) Hanessian, S., Maianti, J. P., Matias, R. D., Feeney, L. A., and Armstrong, E. S. (2011) Hybrid aminoglycoside antibiotics via Tsuji palladium-catalyzed allylic deoxygenation. *Org. Lett. 13*, 6476−6479.

(22) Kahlmeter, G., and Dahlager, J. I. (1984) Aminoglycoside toxicity—A review of clinical studies published between 1975 and 1982. *J. Antimicrob. Chemother. 13* (Suppl A), 9−22.

(23) Chen, L., Hainrichson, M., Bourdetsky, D., Mor, A., Yaron, S., and Baasov, T. (2008) Structure-toxicity relationship of aminoglycosides: correlation of 2′-amine basicity with acute toxicity in pseudodisaccharide scaffolds. *Bioorg. Med. Chem. 16*, 8940−8951.

(24) Mingeot-Leclercq, M. P., and Tulkens, P. M. (1999) Aminoglycosides: nephrotoxicity. *Antimicrob. Agents Chemother. 43*, 1003−1012.

(25) Nudelman, I., Rebibo-Sabbah, A., Cherniavsky, M., Belakhov, V., Hainrichson, M., Chen, F., Schacht, J., Pilch, D. S., Ben-Yosef, T., and Baasov, T. (2009) Development of novel aminoglycoside (NB54) with reduced toxicity and enhanced suppression of disease-causing premature stop mutations. *J. Med. Chem. 52*, 2836−2845.

(26) Kondo, J. (2012) A structural basis for the antibiotic resistance conferred by an A1408G mutation in 16S rRNA and for the antiprotozoal activity of aminoglycosides. *Angew. Chem., Int. Ed. Engl. 51*, 465−468.

(27) Kondo, J., Koganei, M., Maianti, J. P., Ly, V. L., and Hanessian, S. (2013) Crystal structures of a bioactive 6′-hydroxy variant of sisomicin bound to the bacterial and protozoal ribosomal decoding sites. *ChemMedChem 8*, 733−739.

(28) Perez-Fernandez, D., Shcherbakov, D., Matt, T., Leong, N. C., Kudyba, I., Duscha, S., Boukari, H., Patak, R., Dubbaka, S. R., Lang, K., Meyer, M., Akbergenov, R., Freihofer, P., Vaddi, S., Thommes, P., Ramakrishnan, V., Vasella, A., and Bottger, E. C. (2014) 4′-O-substitutions determine selectivity of aminoglycoside antibiotics. *Nat. Commun. 5*, 3112.

(29) Takahashi, Y., Ueda, C., Tsuchiya, T., and Kobayashi, Y. (1993) Study on fluorination-toxicity relationships. Syntheses of 1-N-[(2R,3R)- and (2R,3S)-4-amino-3-fluoro-2-hydroxybutanoyl] derivatives of kanamycins. *Carbohydr. Res. 249*, 57−76.
(30) Morgenthaler, M., Schweizer, E., Hoffmann-Roder, A., Benini, F., Martin, R. E., Jaeschke, G., Wagner, B., Fischer, H., Bendels, S., Zimmerli, D., Schneider, J., Diederich, F., Kansy, M., and Muller, K. (2007) Predicting and tuning physicochemical properties in lead optimization: Amine basicities. *ChemMedChem. 2*, 1100−1115.
(31) Hudlický, M. (1988) Fluorination with diethylaminosulfur rrifluoride and related aminofluorosulfuranes. In *Organic Reactions*, Vol. 35, p 513, John Wiley & Sons, Inc., New York.
(32) Jäger, V., Schröter, D., and Koppenhoefer, B. (1991) Asymmetric sharpless epoxidation of divinylcarbinol. Erythro-D- and -L-4-pentenitols by hydrolysis of regioisomeric epoxy-4-pentenols. *Tetrahedron 47*, 2195−2210.
(33) Kondo, J., Francois, B., Russell, R. J., Murray, J. B., and Westhof, E. (2006) Crystal structure of the bacterial ribosomal decoding site complexed with amikacin containing the γ-amino-α-hydroxybutyryl (haba) group. *Biochimie 88*, 1027−1031.
(34) Armstrong, E. S., Feeney, L. A., Kostrub, C. F. (Achaogen Inc.) Compositions and methods for determining nephrotoxicity, Sept. 3, 2009, US20090220982.
(35) Denamur, S., Van Bambeke, F., Mingeot-Leclercq, M. P., and Tulkens, P. M. (2008) Apoptosis induced by aminoglycosides in LLC-PK1 cells: Comparative study of neomycin, gentamicin, amikacin, and isepamicin using electroporation. *Antimicrob. Agents Chemother. 52*, 2236−2238.
(36) Servais, H., Ortiz, A., Devuyst, O., Denamur, S., Tulkens, P. M., and Mingeot-Leclercq, M. P. (2008) Renal cell apoptosis induced by nephrotoxic drugs: Cellular and molecular mechanisms and potential approaches to modulation. *Apoptosis 13*, 11−32.

NOTE ADDED AFTER ASAP PUBLICATION

This paper was published ASAP on June 14, 2014 with errors in Table 1. The corrected version was reposted on June 17, 2014.